Enhancing and Revealing Hidden Image Details

Madeline Hays

0 | Abstract

This report explores conventional image enhancement techniques for improving degraded images encountered in real-world scenarios, such as surveillance footage. We focus on four primary sources of image degradation: fixed-additive noise, motion blur, poor exposure, and low resolution. Our study evaluates various denoising strategies, including filtering, deconvolution, exposure correction, and super-resolution, using both quantitative (PSNR, SSIM) and qualitative assessments. A subset of images from the BSDS300 dataset was systematically degraded and processed using different enhancement techniques to analyze their effectiveness. Results indicate that the most effective enhancements are highly dependent on the specific noise type, with Gaussian noise filtering and exposure correction providing the most significant improvements. Additionally, we demonstrate that the order of enhancement steps affects final image quality. While conventional methods offer improvements, their reliance on manual parameter tuning presents limitations, suggesting that adaptive optimization and deep learning-based approaches hold promise for future advancements in image restoration and enhancement.

1 | Introduction

The quality of photographic records directly affects their interpretability. While phone cameras have made significant advancements in resolution and HDR contrast, public and commercial security cameras often remain low-quality CCTV systems. These cameras are affected by various forms of image degradation, including weather, lighting conditions, electronic noise, and motion blur [1,2]. Despite these limitations, such footage is critical for law enforcement investigations, where clear images can provide stronger evidence than circumstantial reports [3]. Replacing all surveillance cameras with high-quality alternatives is cost-prohibitive, making image enhancement an essential tool.

Our goal is to examine the interplay between different types of image degradation and conventional enhancement techniques. We investigate how the strategies influence other forms of non-targeted noise as many low-quality images face multiple noise sources. Our aim is to improve image quality while avoiding hallucinated artifacts.

2 | Related work

We address four primary sources of image degradation: fixed-additive noise, motion blur, poor exposure, and low resolution. Each can be mitigated using established image-processing techniques.

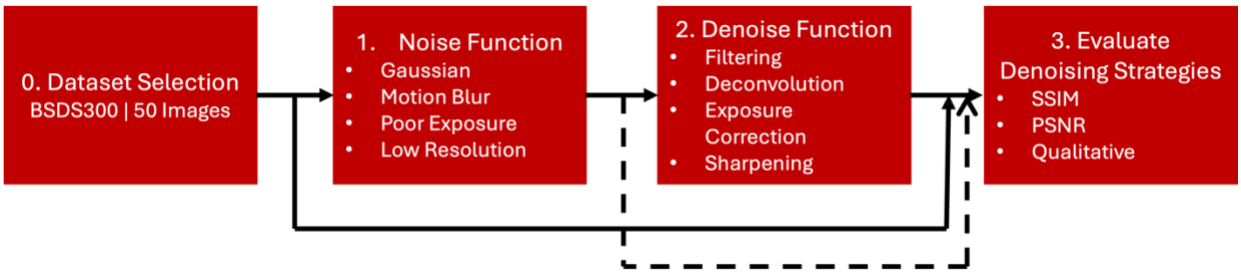

Figure 1. Project Methodology Pipeline

Fixed-additive noise can be modeled as gaussian white noise, commonly originating pixel-to-pixel variations and readout circuitry. Conventional denoising techniques include filters. Gaussian filters provide local, linear smoothing while median filters provide local, non-linear smoothing. Edge preserving filters include anisotropic filters, utilizing a form of orthogonal convolution, and bilateral filters, weighting pixels in local neighborhoods with similar intensities more strongly [4,5]. Block-matching 3D filtering (BM3D) considers patterns within images by grouping blocks of the image by structural similarities. Groups are subjected to discrete cosine transforms followed by thresholding [6].

Motion blur occurs when object move during image capture. Wiener deconvolution attempts to inverse this blur along with an SNR damping factor to allow for the presence of gaussian noise. An alternative method, the Richardson-Lucy (RL) deconvolution assumes a Poisson noise model common in low-light conditions and works iteratively to remove blur [7,8]. However, both these methods assume prior knowledge of the blur kernel. Blind deconvolution techniques iteratively use a normalized sparsity regularizer to optimize a blur kernel estimate [9].

Poor exposure encompasses low-light and overexposed conditions. Tone mapping works to enhance contrast and color by scaling luminance while maintaining high-contrast details. For example, tone mapping with a bilateral filter applies the filter to the intensity information of the image and preserves detail by subtracting the output of the filter from the input when reconciling the image. Tone mapping with a local Laplacian filter uses the logarithmic space to compress the dynamic range of the image while preserving the local contrast [11-13].

Low resolution arises due to limited pixel density in wide-field surveillance cameras. Enhancement methods include unsharp masking, which amplifies high-frequency components, and bicubic interpolation, which smooths pixelation artifacts [14,15].

Figure 2. (a) Clean Image (b) Gaussian Noise (c) Motion Blur (d) Overexposure (e) Underexposure (f) Low Resolution

3 | Method

Our methodology comprises of four key steps (Figure 1).

3.1 | Modeling Noise

To explore these inter-relationships of noise sources and denoising strategies, we first must model the various noise sources (Figure 2).

Gaussian noise was modeled as a white noise added to each pixel (Eq. 1). Levels assessed were σ = [0.1, 0.3, 0.6].

$$I_{noisy}(x,y) = I(x,y) + N(x,y)$$

$$N(x,y) \sim \mathcal{N}(0,\ \sigma) \qquad Eq.\ 1$$

$I(x,y)$ is the original image at pixel (x,y). $N(x,y)$ is the Gaussian noise distributed with mean 0 and standard deviation σ at pixel (x,y).

Motion blur was modeled as a 2D convolutional operation with a normalized horizontal blur matrix (Eq. 2). Levels assessed were N = [5, 10, 20].

$$I_{blurred}(x,y) = (I * K)(x,y)$$

$$K(u,v) = \frac{1}{N}\begin{bmatrix} 0 & \cdots & 0 \\ 1 & \ldots & 1 \\ 0 & \cdots & 0 \end{bmatrix},\ N = size(K) \quad Eq.\ 2$$

K is the blur kernel representing the point spread function.

Poor exposure was modeled as a scaling of pixel intensities where a scale below 1 increased shadows and scale above 1 increased brightness (Eq. 3). The levels for underexposure and overexposure were f = [0.7, 0.5, 0.3] and f = [1.3, 1.6, 2.2], respectively.

$$I_{exp}(x,y) = f \cdot I(x,y)$$

$$Underexposure:\ 0 < f < 1$$

$$Overexposure:\ f > 1 \qquad Eq.\ 3$$

The variable f is the scaling factor.

Low resolution was modeled by applying an anti-aliasing low-pass gaussian filter followed by down-sampling of the image (Eq. 4). The factors of down-sampling were s = [2, 4, 8].

$$I_{lowpass}(x,y) = \sum_{u=-k}^{k}\sum_{v=-k}^{k} I(x-u, y-v)G(u,v,\sigma)$$

$$I_{down}(x',y') = I_{lowpass}(sx', sy')$$

$$G(u,v,\sigma) = \frac{1}{2\pi\sigma^2}e^{-\frac{u^2+v^2}{2\sigma^2}},$$

$$\sigma = \frac{s}{2},\ \ s = scale,\ \ k = radius \qquad Eq.\ 4$$

Where $G(u,v,\sigma)$ is the gaussian filter and (x',y') are the new pixel coordinates.

3.2 | Denoising Strategies

To denoise the images, we investigated strategies of four main categories: filters, deconvolution, exposure correction, and sharpening. All strategies were varying tunable parameters for all noise types at the reported levels.

Filters. Gaussian filters (Eq. 4 - Lowpass) were applied with varying σ from 0.1 to 1.2 in 12 linear steps. Median filters (Eq. 5) were applied with varying kernel sizes, *r*, of 2 to 11 in linear spaces of 1. Bilateral filters [4,5] were applied with a radius of 3, intensity σ of 0.25, and varying spatial σ of 0.3 to 2.4 in 12 linearly spaced steps. Anisotropic filters [5] were applied gradient threshold of 10, step size of 0.15, and varying number of iterations from 5 to 50 in 10 linear steps. Total variation minimization [5] was applied with varying weight of 0.05 to 0.95 in 10 linear steps. Finally, BM3D [6] was applied with varying σ from 0.1 to 0.9 in 9 linear spaced steps.

$$I_{filt}(x,y) =$$

$$\text{median}(\{I(x+i, y+j) \mid -r \le i,j \le r\})\ Eq.\ 5$$

Where the median function selects the median value from neighboring pixels of window size (2r+1) x (2r+1).

Deconvolution. Wiener deconvolution (Eq. 6) and RL deconvolution [7,8]. Kernel sizes were

varied from 2 to 20 in 10 linear steps for both methods.

$$\hat{I}(u,v) = \frac{\widehat{I_b}(u,v)\cdot H^*(u,v)}{|H(u,v)|^2 + S_n(u,v)/S_f(u,v)} \qquad Eq.\ 6$$

Where $\hat{I}(u,v)$ is the FFT of the deconvolved image, $\widehat{I_b}(u,v)$ is the FFT of the noised image, $H(u,v)$ is the optical transform function, and $S(u,v)$ is the power spectral density of the noise and the image, respectively.

Exposure Correction. Adaptive histogram equalization was applied varying the neighborhood size from 2 to 20 in 10 linear steps [10]. Bilateral tone mapping [11] was applied with a spatial σ of 15 and σ range varying from 0.1 to 1 in 10 linear steps. Finally, Laplacian tone mapping [12] was applied. In this function alpha controls contrast and beta controls edge preservation. One set applied set alpha to 1.5 and varied beta from 0.1 to 0.9 in 9 linear steps, and the other set applied set beta to 0.5 and varied alpha from 0.3 to 3 in 10 linear steps.

Low Resolution. A simple implantation of bicubic interpolation [14] was applied varying the scale factor from 2 to 12 in 10 linear steps. Unsharp masking [15] was applied with a σ of 1.5 and varying sharpening strength from 0.5 to 2.5 in 10 linear steps.

3.3 | Evaluation Metrics

For comparison, we have 50 images that were noised with one of 5 noise types at 3 levels of noise per type. To assess denoising strategy performance, we compared peak signal noise ratio (PSNR) and structural similarity index measure (SSIM) between the noised image and the clean image averaged across the dataset to establish a baseline. Denoising strategy performance was evaluated by applying each strategy at the specified parameters to each noised image and calculating the average PSNR and SSIM between the denoised image and the clean image to determine quantitative performance. Then, using the best attempted tuned parameter for either SSIM or PSNR, an example image was displayed for each noise type and level to check perceptual performance.

3.4 | Multi-Noise Processing

Several strategies were attempted to classify a noised image by the noise type. These include peak intensity value, average intensity value, standard deviation of intensities, image skew, and image contrast by percentile difference, blur as average log magnitude of the image FFT, and blur as the Laplacian variance of the image.

Sample images were subjected to multiple noise sources. Denoising strategies were performed in sequence and compared to determine potential impacts on effective image enhancement.

Results

Example results for noised images at the varying levels, denoised image PSNR and SSIM comparison, and denoised images using optimum filter are displayed in the *Appendix*. For full results, see final code

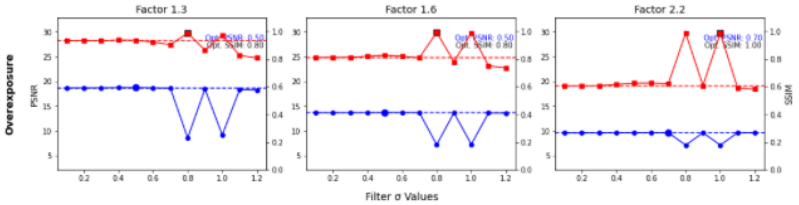

Figure 3 Gaussian Filter performance on 50 overexposed images

Filters. Filters provided the most effective smoothing for Gaussian noise, with BM3D outperforming other methods. However, most filters negatively impact non-Gaussian noise

types with few exceptions. For example, Gaussian filters have the potential to improve SSIM in certain overexposed images but results in a drop in PSNR (Figure 3). Bilateral filtering, while computationally demanding, improves gaussian noise and has the potential to improve motion blur and overexposure given its edge-preserving methods and spatial smoothing, respectively.

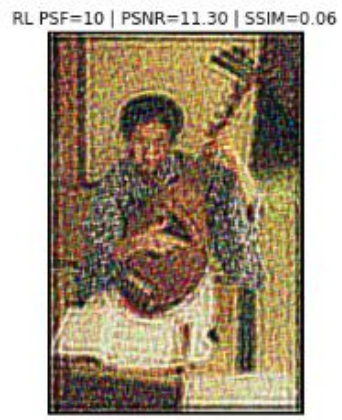

Figure 4 RL Deconvolution on Gaussian Noise (0.3) Image

Deconvolution. Deconvolution did not serve well to the various noise types. Wiener deconvolution had the potential to improve images of gaussian noise but struggled with unknown blur kernels. RL deconvolution can perceptually strengthen edges (Figure 4) but also struggled to improve PSNR and SSIM in noise types including gaussian noise.

Exposure Correction. Adaptive histogram equalization works well on underexposed images of significant degree in both PSNR and SSIM. However, only PSNR improves for mildly significantly overexposed images. For the other noise types, histogram equalization worsens image quality, but larger tile size has a reduced effect. For the bilateral tone mapping, improvement in both PSNR and SSIM is seen for underexposed and overexposed images and worsens all other noise types. For the Laplacian tone mapping, alpha has a larger effect than beta on performance. Of the methods discussed, PSNR and SSIM improve the most for underexposed images. However, there is a more severe effect on other noise types. Contrary to the quantitative measures, many images improve qualitatively with exposure correction strategies (Figure 5). Histogram equalization qualitatively improves most noise types. Bilateral tone mapping improves all except overexposed images and gaussian noise images. Laplacian tone mapping improves poor exposure images better but has less positive qualitative effects on other noise types. The notable exception to consider is certain gaussian noise which can be emphasized in place of the image details. This could result in hallucinated artifacts that are not representative of the true image.

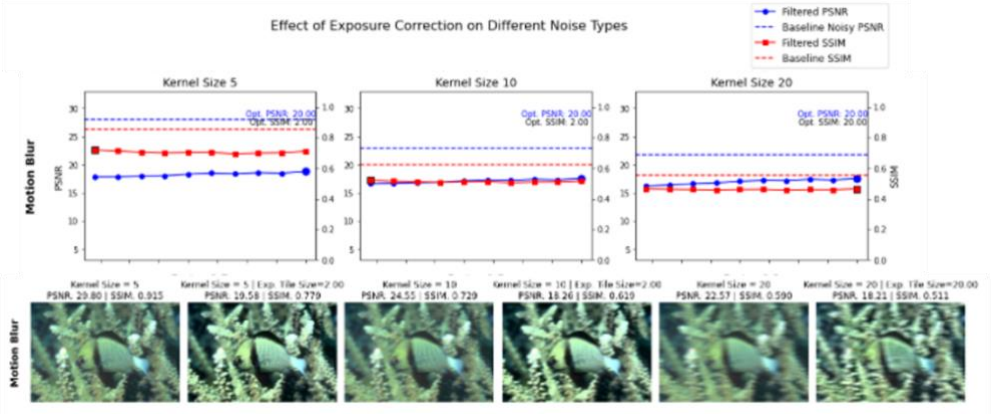

Figure 5. Image Enhancement via adaptive histogram equalization not reflected in quantitative measures

Low Resolution. The simple form of bicubic interpolation applied provides minimal improvement to all noise types. Unsharp masking is the only strategy to show significant improvement in low resolution images in PSNR and SSIM. However, it can significantly impact image quality in other noise types, particularly gaussian noise sharpened by the mask.

Multi-Noise. The most effective measure of poor exposure was average pixel intensity which

is higher for overexposed images (> 125) and lower in underexposed images (< 80). Other correlated but to a lesser degree factors were peak intensity value (overexposed: > 150 and underexposed: < 80). Due to the noise model, overexposed images also featured a larger standard deviation (> 50) while underexposed images had a lower standard deviation (< 40). Gaussian noise exclusively had a high standard deviation (> 50). Skew and contrast were not reliable metrics to identify noise types as trends hold within an image, but variability is high across images. Low resolution and motion blurred images have a low FFT defined blur (< 7) and a low Laplacian variance (< 400). Low resolution images were particularly identifiable with lower values (FFT blur: < 6 and Laplacian blur: < 40).

When it comes to applying denoising strategies, the noise sources matter to the application of which strategies and when. For an order of application example, in an image with low resolution, motion blur, gaussian noise, and underexposure, it is more effective to denoise via BM3D followed by adaptive histogram equalization than vice versa (Figure 6). Further image enhancement steps only marginally improve the image.

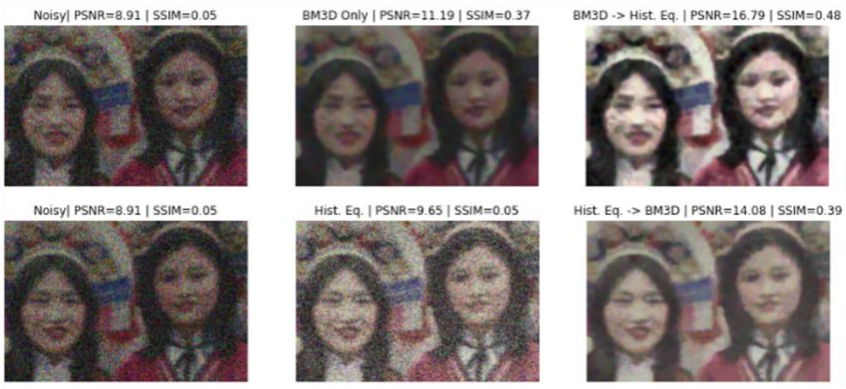

Figure 6. Comparison of order of denoising strategies to image with 4 noise sources (low resolution, underexposure, gaussian, motion blur)

Discussion

From our results, we can tell that denoising strategies are highly effective against their targeted noise type but can inadvertently degrade image quality when applied to non-targeted distortions. Identifying noise sources is critical for effective application of conventional denoising strategies like the ones explored here. Furthermore, methods perform best in a particular order dependent on the image and the strategies chosen. From our results, the largest enhancements can be obtained via gaussian noise removal and exposure correction. Tone mapping can reveal hidden features in images if the quality starts at a reasonable threshold.

There are several limitations to this work. First, only conventional methods of image enhancement were tried without CNNs. CNNs greatly expand the possibilities for this work, particularly if they can either be trained on a variety of noisy data or have the different denoising strategies tuned in separate stages (for example, wiener deconvolution + CNN denoiser performing better than the CNN alone). All the methods discuss, while straightforward to implement, also suffer from needing manual input of parameters. Preferably, these parameters would be chosen based on noise measurements and strategies chosen. Importantly, exposure correction methods enhance aspects of the image (edges, contrast), revealing background details previously obscured. Image enhancement holds promise for improving CCTV images but cannot be captured quantitatively by PSNR or SSIM as the image is differentiated from the original.

Ideally to move this work forward we would want to create a comprehensive model of the different noise types when stacked. Further, we may want to consider Poisson noise in low light conditions or refractive noise from weather events such as rain or snow. We would then want to format a convex optimization objective to quickly and decisively tune parameters for image improvement. Realistically, CNN's and other optimizing algorithms hold the most promise for this work as it can better treat individual images [16-21]. For example, motion kernels can be estimated by image patch and edge detection is often inherent in CNN layers.

References

[1] Pinson, M. H. (2017). *Gaps in Public-Safety Cameras: How dust, rain, snow, and shadows impact public safety video*. MissionCritical Communications. Retrieved from

[2] Sirix Monitoring. (2024). *Why are security cameras so low quality?* Retrieved from

[3] San Francisco Police Department. (2022). *Surveillance Impact Report: Non-City Entity Surveillance Cameras*. Retrieved from

[4] A. Buades, J. M. Morel, "A Non-Local Algorithm for Image Denoising," Proceedings of IEEE Conference on Computer Vision and Pattern Recognition (CVPR), 2005.

[5] S. Paris, P. Kornprobst, J. Tumblin, F. Durand, "A Gentle Introduction to Bilateral Filtering and its Applications," SIGGRAPH 2007 Course Notes.

[6] K. Dabov, A. Foi, V. Katkovnik, K. Egiazarian, "Image Denoising by Sparse 3D Transform-Domain Collaborative Filtering," IEEE Transactions on Image Processing, vol. 16, no. 8, pp. 2080-2095, 2007.

[7] W. H. Richardson, "Bayesian-Based Iterative Method of Image Restoration," Journal of the Optical Society of America, vol. 62, no. 1, pp. 55–59, 1972.

[8] L. B. Lucy, "An Iterative Technique for the Rectification of Observed Distributions," The Astronomical Journal, vol. 79, p. 745, 1974.

[9] D. Krishnan, T. Tay, R. Fergus, "Blind Deconvolution Using a Normalized Sparsity Measure," IEEE Conference on Computer Vision and Pattern Recognition (CVPR), 2011.

[10] Pizer, S. M., Amburn, E. P., Austin, J. D., Cromartie, R., Geselowitz, A., Greer, T., ... & Zimmerman, J. B. (1987). Adaptive histogram equalization and its variations. *Computer Vision, Graphics, and Image Processing*, 39(3), 355-368.

[11] F. Durand, J. Dorsey, "Fast Bilateral Filtering for the Display of High Dynamic Range Images," ACM SIGGRAPH, 2002.

[12] S. Paris, S. Hasinoff, J. Kautz, "Local Laplacian Filters: Edge-Aware Image Processing with a Laplacian Pyramid," ACM Transactions on Graphics (TOG), Proceedings of SIGGRAPH, 2011.

[13] Z. Farbman, R. Fattal, D. Lischinski, R. Szeliski, "Edge-Preserving Decompositions for Multi-Scale Tone and Detail Manipulation," ACM Transactions on Graphics (TOG), Proceedings of SIGGRAPH, 2008.

[14] Khaledyan, D., Amirany, A., Jafari, K., Moaiyeri, M. H., Zargari Khuzani, A., & Mashhadi, N. (2020). *Low-Cost Implementation of Bilinear and Bicubic Image Interpolation for Real-Time Image Super-Resolution*. arXiv preprint arXiv:2009.09622. Retrieved from

[15] Trussell, H. J., & Hartwig, R. E. (1974). *Mathematics for the Generalized Unsharp Masking Operator*. Computer Graphics and Image Processing, 3(3), 256-267.

[16] C. A. Metzler, H. Heidari, F. Heide, G. Wetzstein, "Deep Optics for Single-Shot High-Dynamic-Range Imaging," Proceedings of IEEE Conference on Computer Vision and Pattern Recognition (CVPR), 2020.

[17] K. Zhang, W. Zuo, Y. Chen, D. Meng, L. Zhang, "Beyond a Gaussian Denoiser: Residual Learning of Deep CNN for Image Denoising," IEEE Transactions on Image Processing, vol. 26, no. 7, pp. 3142–3155, 2017.

[18] B. Lim, S. Son, H. Kim, S. Nah, K. M. Lee, "Enhanced Deep Residual Networks for Single Image Super-Resolution," Proceedings of IEEE Conference on Computer Vision and Pattern Recognition (CVPR) Workshops, 2017.

[19] D. Geman, C. Yang, "Nonlinear Image Recovery with Half-Quadratic Regularization," IEEE

Transactions on Image Processing, vol. 4, no. 10, pp. 932–946, 1995.
[20] S. Boyd, N. Parikh, E. Chu, B. Peleato, J. Eckstein, “Distributed Optimization and Statistical Learning via the Alternating Direction Method of Multipliers,” Foundations and Trends in Machine Learning, vol. 3, no. 1, pp. 1–122, 2011.
[21] L. Rudin, S. Osher, E. Fatemi, “Nonlinear Total Variation-Based Noise Removal Algorithm,” Physica D: Nonlinear Phenomena, vol. 60, no. 1-4, pp. 259-268, 1992.

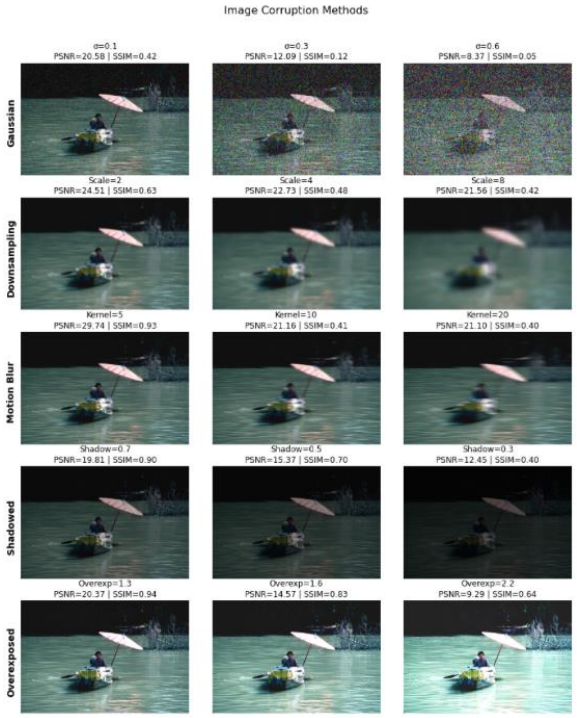

Appendix 1. Five Noise Types at 3 Levels of Severity

Appendix

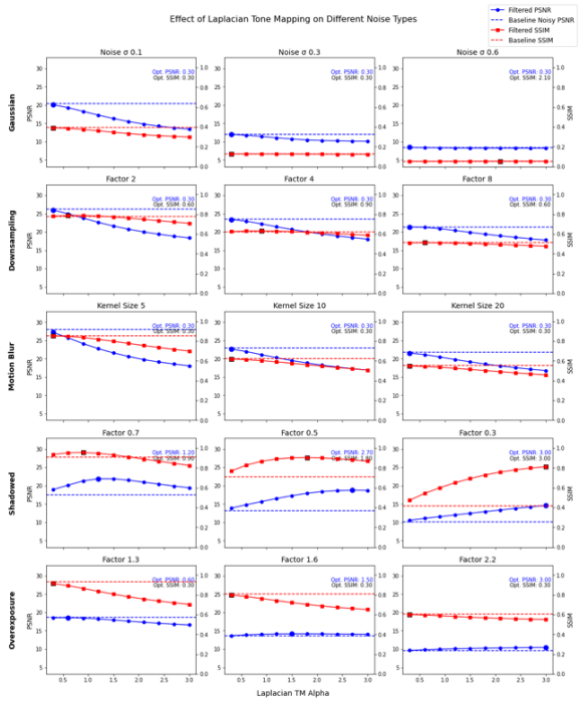

Appendix 2. PSNR & SSIM Comparison for Laplacian Tone Mapping on all Noise Types and levels, varying tunable parameter alpha

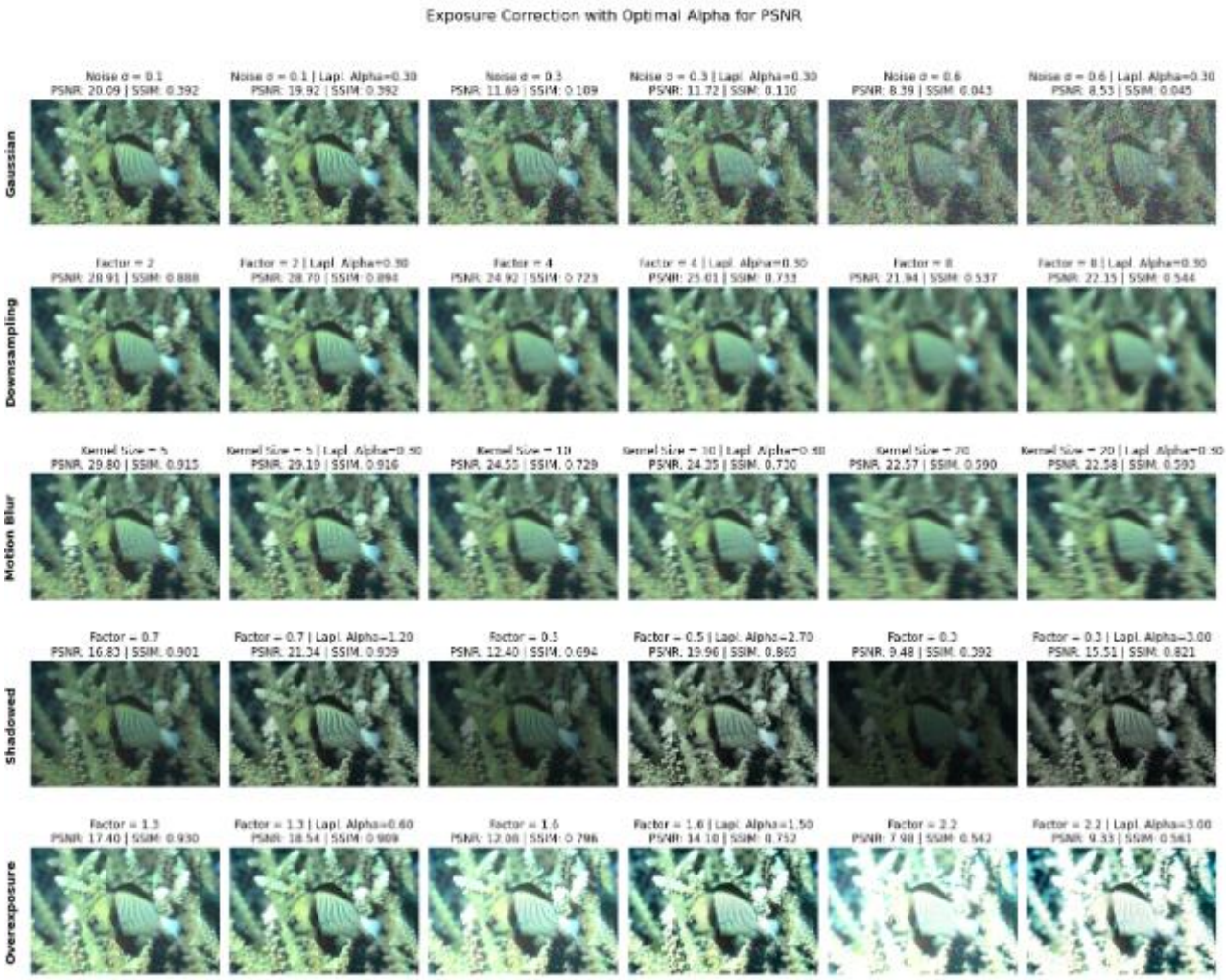

Appendix 3 Qualitative Comparisons for Laplacian Tone Mapping